EurJIC
European Journal of Inorganic Chemistry

Research Article
doi.org/10.1002/ejic.202300288

Chemistry Europe
European Chemical Societies Publishing

www.eurjic.org

VIP *Very Important Paper*

Special Collection

Lanthanide-FRET Molecular Beacons for microRNA Biosensing, Logic Operations, and Physical Unclonable Functions

Mariia Dekaliuk*[a, b] and Niko Hildebrandt*[a, c, d]

Time-resolved or time-gated (TG) biosensing and bioimaging with luminescent lanthanide probes and Förster resonance energy transfer (FRET) have significantly advanced bioanalytical chemistry. However, the development of lanthanide-based molecular beacons (MBs) has been rather limited. Here, we designed DNA stem-loop MB probes against two different microRNAs (miR-21 and miR-27b) using Tb and Eu FRET donors and quenching (BHQ2) and fluorescent (Cy3) FRET acceptors. Limits of detection down to 190 pM and duplexed miR-21/miR-27b quantification at low nanomolar concentrations with Tb-BHQ2 and Eu-BHQ2 TG-FRET MBs demonstrated the versatility and high analytical performance of lanthanide-based MBs. The particular donor-acceptor distances in the Tb-Cy3 MB resulted in inverted nucleic acid target concentration-dependent TG PL intensities in short (e.g., 0 to 40 μs) and long (e.g., 0.1 to 2.1 ms) TG detection windows after pulsed excitation. We showed that this specific feature of our TG-FRET MBs can be adapted to the design of molecular logic devices (NOR, OR, NAND, AND, XNOR, XOR, IMPLEMENT, and INHIBIT). Moreover, the almost unlimited choice of TG detection windows and the distinct spectral features of Tb and Cy3 over a broad visible spectral range could be exploited to devise biophotonic physical unclonable functions for highly secure authentication and identification. Our study manifests the versatility of lanthanides for advanced biophotonic applications.

Introduction

Förster resonance energy transfer (FRET) is a frequently used technique to analyze biomolecular interactions via photoluminescence (PL) spectroscopy or microscopy.[1–5] Conventional FRET pairs consist of fluorescent dyes, proteins, or nanoparticles as donors and/or acceptors and non-fluorescent small molecular quenchers as acceptors.[6] Gold nanoparticles are also frequently applied as quenching acceptors in resonance energy transfer. However, the quenching mechanism (nanosurface energy transfer – NSET) is slightly different from FRET.[7] The long PL lifetimes, broad PL spectra with several narrow and well-separated emission peaks, large wavelength gaps between excitation and emission, and high photostability of lanthanides (ions, complexes, or nanoparticles) are ideally suited for their application in PL biosensing and bioimaging.[8–17] Suppression of autofluorescence background from biological samples by time-resolved or time-gated (TG) detection and ratiometric sensing via detection of both FRET donor and acceptor emission are only two of the important advantages of lanthanides for bioanalysis. Lanthanides are almost exclusively used as FRET donors because their very long excited-state lifetimes (up to milliseconds) are not ideal for efficiently accepting energy from the usually much shorter lived excited states (usually nanoseconds) of other luminescent materials.[4,18–20] It should be noted that lanthanide ions can also be energy acceptors when they are coordinated by organic ligands.[21] In this so-called antenna effect, the lanthanide ion is sensitized via the triplet state of the ligand.[22] However, considering the short distance between ligand and lanthanide, it is not clear if the energy transfer mechanism is Dexter energy transfer or FRET.[23]

Many lanthanide-based TG-FRET assays have been developed,[4] including commercial tests, such as *LANCE*, *HTRF*, *THUNDER*, *TRACE*, or *TruPoint*.[24–29] One recent focus of TG-FRET has been its implementation into DNA biosensing, including the application of DNA aptamers for histamine quantification,[30] DNA-DNA hybridization for multiplexed sensing and the development of molecular logic devices,[19,31–33] or DNA amplification for the quantification of extremely low concentrations of

[a] *Dr. M. Dekaliuk, Prof. Dr. N. Hildebrandt*
nanoFRET.com, Laboratoire COBRA (UMR6014 & FR3038)
Université de Rouen Normandie, CNRS, INSA, Normandie Université
76000 Rouen (France)

[b] *Dr. M. Dekaliuk*
Department of Molecular Probes and Prodrugs, Institute of Bioorganic Chemistry
Polish Academy of Sciences
61-704 Poznan (Poland)
E-mail: mdekaliuk@ibch.poznan.pl

[c] *Prof. Dr. N. Hildebrandt*
Department of Chemistry
Seoul National University
Seoul 08826 (South Korea)

[d] *Prof. Dr. N. Hildebrandt*
McMaster University
Department of Engineering Physics
1280 Main Street West, Hamilton, L8S 4L7 (Canada)
E-mail: hildebrandt@mcmaster.ca
Homepage: www.nanofret.com

Supporting information for this article is available on the WWW under https://doi.org/10.1002/ejic.202300288

Special Collection *Part of the "Chemistry and Applications of the f-Block Elements" Special Collection.*

Research Article
doi.org/10.1002/ejic.202300288

DNA and RNA targets.[34–39] Molecular beacons (MBs) are specific DNA FRET probes that form hairpin structures via intramolecular base-pairing, such that the 3′ and 5′ termini of the DNA are adjacent. The termini are labeled with a FRET donor and acceptor (usually a quencher), respectively, which results in very efficient FRET in the closed hairpin configuration and inefficient or no FRET when the hairpin is opened via target hybridization. This relatively simple but very smart biosensing approach was developed more than 25 years ago and has been used in a myriad of different biosensing applications in research and molecular diagnostics.[40,41] Lanthanides, including Tb, Eu, Dy, and Sm have also been applied as FRET donors in MBs (or similar structures) for the detection of single-stranded (ss)DNA targets.[42–47] Although the application potential of such lanthanide-based TG-FRET MBs is in principle much broader than sensitive quantification of ssDNA, multiplexing with different lanthanides, quantification of RNA biomarkers, Boolean logic operations, or security encryption have not been realized so far.

Motivated by the current limitations of TG-FRET MBs, we aimed at broadening their application range to a combination of Tb and Eu donors with molecular quenchers and fluorescent dye acceptors for multiplexed quantification of microRNAs (miRNAs), molecular logic devices (MLDs), and physical unclonable functions (PUFs). Using simple and rapid time-gated PL measurements on a commercial benchtop fluorescence plate reader, we demonstrate that the TG-FRET MBs are applicable to multiplexed miRNA sensing and that target concentration-dependent analysis in specific TG detection windows can be used to design logic operations and PUFs. Our results illustrate how lanthanides can significantly extend the application range of established molecular probes and demonstrate the broad applicability of TG-FRET MBs for biosensing, biocomputing, and biophotonic security, authentication, and identification.

Results and Discussion

Molecular beacon design and experimental conditions

The recognition principle of MB probes is based on complementary stacking and pairing with specific target nucleic acids (e.g., miRNA or ssDNA). We designed two different MB probes that can complementarily recognize two different target miRNAs, namely miR-21 and miR-27b. The oligonucleotide sequences of the two MBs were based on previously published MBs with dye-quencher FRET pairs, which demonstrated high selectivity and sensitivity to these miR targets.[48] The MB probes consisted of 28 to 30 nucleotides (nt) including 5 to 6 nt of stem and 18 to 20 nt of loop sequences (cf. Table 1 for sequences of all oligonucleotides used in this study). The 3′ termini of the MBs were readily functionalized (provided by the supplier) with the fluorescent dye Cy3 or the PL quenching molecule Black Hole Quencher 2 (BHQ2) as FRET acceptors, whereas the 5′ termini were bioconjugated in-house with Lumi4-Tb (Tb) or Lumi804-Eu (Eu) FRET donors via amino groups on the MB and N-hydroxysuccinimide (NHS) ester groups on Tb and Eu. Based on the spectral overlap of donor emission and acceptor absorption (Figure 1A), the possible FRET pairs were Tb-Cy3, Tb-BHQ2, and Eu-BHQ2. Förster distances (R_0, donor-acceptor distance for which FRET efficiency is 50 %) of R_0(Tb-BHQ2) = 5.7 ± 0.3 nm, R_0(Eu-BHQ2) = 5.7 ± 0.3 nm, and R_0(Tb-Cy3) = 6.6 ± 0.4 nm were calculated using Equations (1) and (2) (Experimental Section).

The absence/presence of a MB-specific target results in a closed/open conformation and thus, different FRET scenarios (Figure 1B). In the closed state, donor and acceptor are in close proximity, which leads to very efficient FRET. In the open state, donor and acceptor are separated by double-stranded (ds)DNA of 21 or 22 nt (depending on the target), the remaining ssDNA termini of 7 or 8 remaining nt (depending on the target), and the C_6 spacer to which the Tb and Eu donors were bioconjugated. The relatively rigid dsDNA should lead to a separation of ~6.9 nm and ~7.3 nm, respectively, when considering a distance of 0.33 nm per basepair.[49] The ssDNA and C_6 linker termini are relatively flexible, which should in principle not extend the overall average separation distance. Whereas the exact value of the donor-acceptor distance is of minor importance, it should be in a range, where FRET is still possible but significantly less efficient (e.g., a distance of $R = 7.3$ nm and $R_0 = 6.6$ nm for the Tb-Cy3 FRET pair would lead to a FRET efficiency of $E_{FRET} = R_0^6/(R_0^6 + R^6) = 0.35$). For the Tb-BHQ2 and Eu-BHQ2 FRET pairs, the different FRET efficiencies should lead to efficient Tb/Eu PL quenching in the closed and relatively strong Tb/Eu PL in the open state, i.e., increasing Tb/Eu PL intensities with increasing target concentrations. For the Tb-Cy3 FRET pair, the closed/open state should result in strong/weak

Table 1. Sequences and modifications of all oligonucleotides used in this study. Complementary sequences are shown in bold letters. Internal names present the laboratory nomenclature for the oligonucleotides.

Probe name	Sequence 5′-3′	Modification	Internal name
Tb-BHQ2 miR-21 Eu-BHQ2 miR-21	AGCG**TCAACATCAGTCTGATAAGCTA**CGCT	5′-C_6 amino 3′-BHQ2	*NBP687*
Tb-BHQ2 miR-27b	C**GCAGAACTTAGCCACTGTGAA**TCTGCG	5′- C_6 amino 3′-BHQ2	*NBP702*
Tb-Cy3 miR-21	AGCG**TCAACATCAGTCTGATAAGCTA**CGCT	5′- C_6 amino 3′-Cy3	*NBP697*
has-miR-21-5p (miR-21)	**UAGCUUAUCAGACUGAUGUUGA**	N/A	*NBP179*
has-miR-27b–3p (miR-27b)	**UUCACAGUGGCUAAGUUCUGC**	N/A	*NBP703*

Research Article
doi.org/10.1002/ejic.202300288

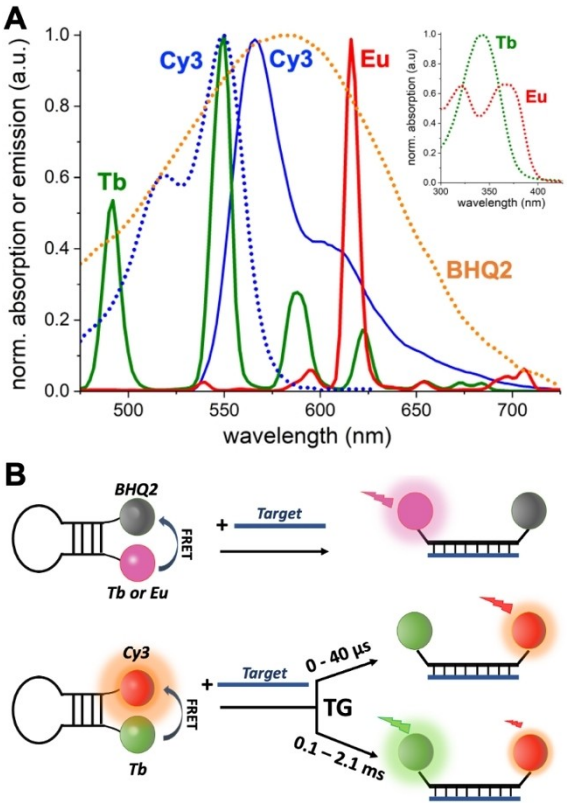

Figure 1. A) Absorption (dotted lines) and emission (solid lines) spectra of the fluorophores used in this study (inset shows Tb and Eu absorption spectra). B) Schematic representation of two types of TG-FRET MB probes with Tb-BHQ2 and Eu-BHQ2 (top) and Tb-Cy3 (bottom) in the closed (without target, left) and open (with target, right) conformational states. Relatively weak FRET ($E_{FRET} < 0.5$) in the case of the Tb-Cy3 MB leads to TG PL intensities of Tb and Cy3 that depend on the TG detection window (delay and gate times). The example on the bottom right shows a short TG window (0–40 µs after the excitation pulse), which results mainly in Cy3 PL detection, and a long TG window (0.1–2.1 ms after the excitation pulse), which results mainly in Tb PL detection.

Tb PL quenching and Cy3 PL sensitization. Thus, a ratiometric assay with increasing Cy3-to-Tb PL intensity ratio with increasing target concentration should in principle be possible.

Single FRET-pair assay performance

The analytical performance of the different TG-FRET MB probes was evaluated on a SPARK (Tecan) benchtop fluorescence plate reader by using miR-21 (for all three MBs) and miR-27b (for Tb-BHQ2) as prototypical targets and a TG detection window of 0.1 to 2.1 ms after pulsed excitation. Because the conformation and target hybridization of MBs is temperature dependent, we first performed optimization experiments. Whereas even simple room temperature conditions resulted in excellent assay conditions, heating to 65 °C followed by slow temperature decrease to 22 °C provided the best assay performance (Figure S1). To determine sensitivities and limits of detection (LOD) of the different MB probes, we recorded assay calibration curves that displayed the Tb or Eu donor TG PL intensity or the Cy3-to-Tb TG PL intensity ratio over target concentration in a range from 0.25 to 50 nM. All four MBs showed a clear target concentration-dependent signal increase (Figure 2). As expected from the already target-optimized MBs,[48] no significant signal change was detectable for non-target controls (miR-27b instead of miR-21 and vice versa), which confirmed the target selectivity of the assays.

Whereas the quencher-based TG-FRET MBs showed an approximately linear signal increase over the tested target concentration range, the Tb-Cy3 TG-FRET MB displayed a steep linear signal increase only until circa 10 nM, which leveled off for higher concentrations. This signal saturation was most probably caused by a combination of ratiometric detection (which calculates the FRET ratio from TG Cy3 and Tb emission) and the higher FRET efficiency (larger R_0) of the Tb-Cy3 FRET pair compared to the Tb-BHQ2 and Eu-BHQ2 MBs, which led to less signal change for the same configurational change of the MB. The different assay performance of the two Tb-BHQ2 MBs (for miR-21 and miR-27b detection) is interesting, because it shows that the sensitivity of a MB probe is not only dependent on the FRET pair but also on the donor-acceptor distance change upon switching from the closed to the open state as well as the MB sequence. The MB for miR-27b detection is 2 nt shorter than the MB for miR-21 detection (and miR-27b is 1 nt shorter than miR-21), which means that the signal change (from closed to open) will be less significant. The different sequence and thus, target-hybridization efficiency, is also influencing the assay performance. However, based on our results, it is impossible to state which of the two (distance change or sequence) had more influence on assay performance. Finally, the Tb-BHQ2 and Eu-BHQ2 MBs show slight differences in their miR-21 assay performance despite the same MB and the same R_0 for both FRET pairs. The higher sensitivity of the Tb-BHQ2 MB

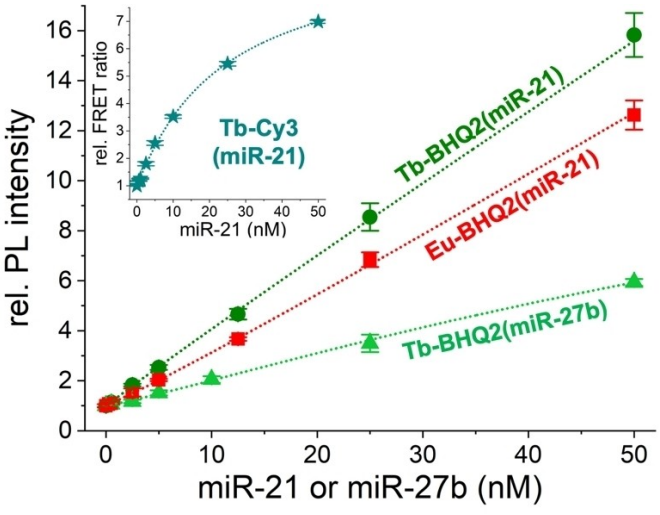

Figure 2. Assay calibration curves for the different TG-FRET MBs. TG PL intensities were measured at the peak wavelengths of 494 nm, 570 nm, and 620 nm for Tb, Cy3, and Eu, respectively (cf. Figure 1A). The Tb-Cy3 MB was used as a ratiometric assay, which analyzed the TG PL intensity ratio (cf. equation 4 in the experimental section) of Cy3 and Tb (inset). Target concentrations correspond to the concentrations in the total assay volume of 100 µL.

Research Article
doi.org/10.1002/ejic.202300288

is most probably related to the higher brightness of Tb (both higher molar extinction coefficient and higher quantum yield) compared to Eu. The PL decay curves of the Tb and Eu donors provide good evidence for the different target concentration-dependent PL behaviors of the distinct MB probes (Figure S2).

The assay sensitivities (*S*) present the slopes of the linear parts of the calibration curves and were: *S*(Tb-BHQ2; miR-21) = 0.34 ± 0.04 nM^{-1}, *S*(Eu-BHQ2; miR-21) = 0.27 ± 0.03 nM^{-1}, *S*(Tb-BHQ2; miR-27b) = 0.14 ± 0.02 nM^{-1}, and *S*(Tb-Cy3; miR-21) = 0.51 ± 0.05 nM^{-1}. LODs were determined as the concentrations on the assay calibration curves that showed a signal with 3 standard deviations above the zero control (Figure S3) and were: *LOD*(Tb-BHQ2; miR-21) = 0.42 ± 0.04 nM (i.e., 42 ± 4 fmol in 100 μL), *LOD* (Eu-BHQ2; miR-21) = 0.83 ± 0.08 nM (i.e., 83 ± 8 fmol in 100 μL), *LOD* (Tb-BHQ2; miR-27b) = 1.9 ± 0.2 nM (i.e., 190 ± 20 fmol in 100 μL), and *LOD* (Tb-Cy3; miR-21) = 0.19 ± 0.02 nM (i.e., 19 ± 2 fmol in 100 μL). It should be noted that the molar LODs in the actual sample (the assay volume of 100 μL contains 25 μL of sample and 75 μL of assay reagents) are four times higher. Whereas comparison of sensitivities and LODs is not necessarily meaningful if assays were performed and analyzed under different conditions and used different targets, the assay performance parameters of our TG-FRET MBs correspond well to those found for the same MBs and miRNA targets[48] and for other lanthanide-based MBs but with different targets,[42–47] all of which were also able to quantify targets in the low to sub nanomolar concentration range.

In order to demonstrate the applicability of our TG-FRET MB probes for target detection in more challenging environment, e.g., serum or plasma samples used in clinical diagnostics, we tested the Tb-BHQ2-miR-21 assay with different fractions of newborn calf serum (NBCS). Even the addition of 25 μL of NBCS to the assay (which corresponded to 100% of serum in the actual 25 μL sample) reduced the assay performance only slightly (Figure S4), which demonstrated that the TG-FRET MB probes are well suited for miRNA quantification also under more challenging biological or clinical conditions.

Duplexed miRNA assay

In addition to the quantification of RNA targets with lanthanide-based TG MBs, we also wanted to demonstrate that two different lanthanides donors using the same quencher as acceptor can be applied for multiplexed target detection. Because both Eu and Tb can be excited at the same wavelength (e.g., 337 nm) and detected at well-distinguishable wavelengths (e.g., 620 nm for Eu and 550 nm for Tb), we applied the two Eu-BHQ2-miR-21 and Tb-BHQ2-miR-27b TG-FRET MBs in a duplexed assay format. Five different assay mixtures containing both MB probes and 1, 5, 10, 25, and 50 nM of each miR-21 and miR-27b were prepared and TG PL intensities (0.1 to 1.1 ms) of Eu (620 nm emission peak) and Tb (550 nm emission peak) were measured on the SPARK plate reader. The spectral overlap of Tb and Eu PL at 620 nm (cf. Figure 1A) required Eu signal correction by a crosstalk correction factor of 0.755 (see Experimental Section). To avoid spectral crosstalk, it would have also been possible to measure the Eu PL around 700 nm, which is free of Tb PL. However, we selected the 620 nm Eu emission peak because it was significantly more intense and provided a better spectral overlap with the BHQ2 acceptor (cf. Figure 1A). The spectral overlap of Tb and Eu at 550 nm was negligible (crosstalk correction factor of 0.998), such that Tb did not require crosstalk correction. Despite the lower spectral crosstalk at 550 nm, the Tb-based MB probe showed larger errors (Figure 3 right), which was caused by the significantly lower

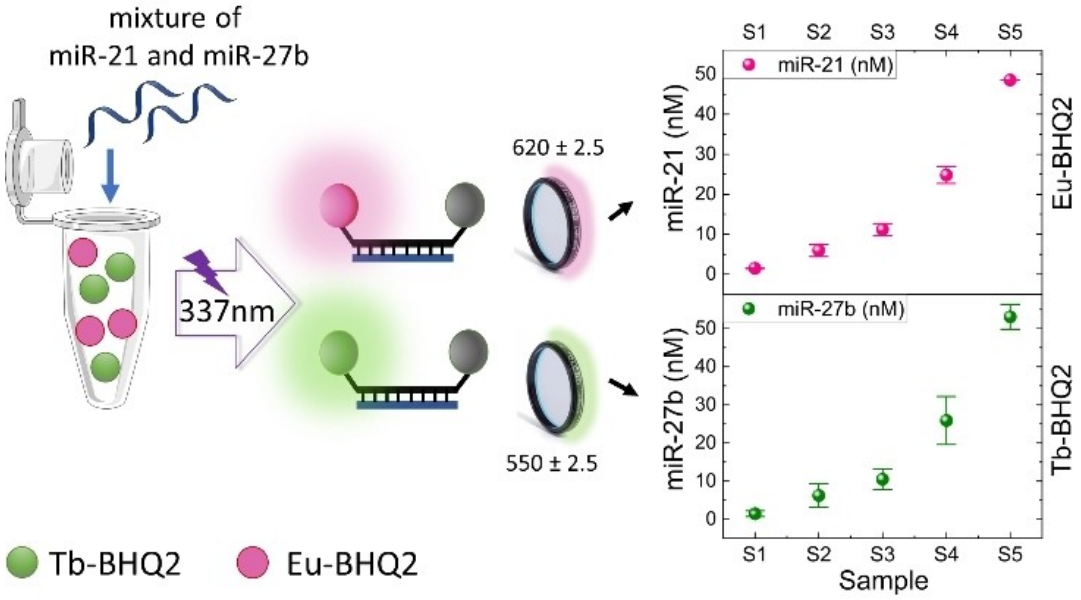

Figure 3. Assay principle (left) and target quantification in five different samples (S1 to S5, right) of a duplexed TG-FRET miRNA assay with two Tb and Eu based MB probes. Each sample contained an equal concentration of both targets (miR-21/miR-27b ratio = 1/1) with concentrations of 1, 5, 10, 25, and 50 nM, respectively.

sensitivity and higher LOD of the miR-27b MB probe (cf. calibration curves in Figure 2). Nevertheless, the duplexed miR-21/miR-27b assay could quantify both targets in the different samples with only minor deviations (within 10%) from the actual target concentrations (Figure 3), which demonstrated the applicability of the two Eu and Tb TG-FRET MB probes for multiplexed miRNA quantification at low nanomolar concentrations.

Specific time-gated FRET detection for logic operations

One intriguing aspect of the TG-FRET MBs is their different PL decay behavior upon target hybridization (Figure S2). In particular, the Tb-Cy3 FRET pair shows multiexponential PL decays despite the fact that there are only two distance configurations, namely closed and open. It is important to note that MB probes are usually employed for off-on PL detection because the closed MB brings donor and acceptor in a very close proximity, such that the donor PL is efficiently quenched (PL off) and the open MB separates donor and acceptor, such that the donor PL is recovered (PL on). If a fluorescent acceptor is used, the on-off PL situation is inverted (acceptor PL on in the closed and off in the open state). For TG-FRET with lanthanide donors, MBs can lead to the peculiar situation that FRET in the closed state is so efficient that both the FRET-quenched donor PL decay time and the FRET-sensitized acceptor PL decay time become very short and can therefore not be detected by longer TG detection windows. Finding a good donor-acceptor distance for a specific TG detection window was previously coined "sweet spot" by Algar at al.[32]

In contrast to the "sweet spot" concept for finding the ideal donor-acceptor distance for practical use of TG-FRET, our Tb-Cy3 TG-FRET MB with very efficient FRET in the closed and low to medium efficient FRET in the open state enables more of a "sweep spot" concept, for which a signal can be simultaneously swept in one specific TG detection window and swept off another by changing the target concentration. In the closed state, Tb-to-Cy3 is so efficient that the PL of FRET-quenched Tb and FRET-sensitized Cy3 are very weak in long TG detection windows, whereas Cy3 PL is strongly dominant in short TG detection windows. In the open state, the low to medium FRET efficiency only slightly quenches/sensitizes Tb/Cy3 PL intensity and decay time and Tb PL is dominant in long TG detection windows, whereas Cy3 PL is very weak in short TG detection windows. The overall situation is particularly interesting because the emission of Tb and Cy3 cover the same spectral range (from ca. 450 to 750 nm) but with specific Tb or Cy3 spectral signatures (Figure S5). Considering that the Tb PL decays over approximately 10 ms (Figure S2), an almost unlimited amount of distinct TG detection windows is available (all from the same TG-FRET MB). All these windows have specific spectral and intensity contributions of both Tb donor and Cy3 acceptor that can be exploited for designing specific target concentration-dependent PL intensity curves with specific increasing or decreasing PL intensity directions.

An example is shown in Figure 4A (short TG detection window from 0 to 40 μs) and Figure 4B (long TG detection window from 0.1 to 2.1 ms). For these two TG detection windows the same target concentration-dependent measurement resulted in simultaneously decreasing short (Figure 4C) and increasing long (Figure 4D) TG PL intensities with increasing target concentration. Within such target concentration-dependent PL intensity curves, different intensity thresholds can be used to define "ON" (or "1") and "OFF" (or "0") states that can be used for logic operations. Both the biological and the biophotonic nature of the TG-FRET MB can in principle be exploited for designing a large variety of logic gates because inputs and outputs can be (bio)chemical, including oligonucleotides (DNA and RNA) and ions (i.e., salt concentration in the buffer solution), and/or physical, including wavelength (color), time (excitation time, detection time, and PL lifetime), temperature, and intensity (TG and continuous wave intensities).

Molecular logic devices (MLDs)

Using the above-mentioned advantages of TG-FRET MBs to create specific on and off PL thresholds, we can design MLDs with nucleotides (DNA) as input and TG PL intensities as output. By selecting different TG detection windows, our TG-FRET MBs can be used for eight different MLDs (NOR, OR, NAND, AND, XNOR, XOR, IMPLEMENT, and INHIBIT) with only four different configurations. For illustrating the different TG-FRET MB MLD capabilities, we applied the MLD principles developed by Park et al.[50] The MLDs from Park's study used relatively short DNA MBs (24 nucleotides), a short PL lifetime dye as FRET donor, and a non-luminescent quencher as FRET acceptor. The eight discussed MLDs required eight different configurations. Detection was conventional continuous-wave PL intensity detection of the donor PL only. Whereas the same input concept can be used for our TG-FRET MDLs, the TG-FRET output strategy (with different TG detection windows instead of different biochemical configurations) is significantly simpler. It is worth mentioning that TG-FRET was previously used to design MLDs, for which Tb and dye labeled peptides were used as inputs.[51] Both peptides self-assembled to semiconductor quantum dots (QDs) via hexahistidine tags, which resulted in specific PL intensities for TG and continuous-wave detection that was used for the development of biophotonic MLDs. Whereas our output concept with two different TG detection windows is somewhat similar to the Tb-QD-dye FRET approach, the simple opening of the MB is significantly more facile compared to dual peptide attachment to QDs.

For all MLDs, we considered the same input strategy as in the dye-quencher MBs from Park et al.,[50] namely two different oligonucleotides (A and B) as biochemical inputs, such that specific hybridization with the MBs would result in a closed or open MB. The short (0–40 μs) or the long (0.1–2.1 ms) TG detection windows were considered as outputs. Input "0" was defined as no DNA (zero concentration of A or B) and input "1" was defined as 200 nM of DNA A or B. The output thresholds (between "0" and "1") were defined as specific TG PL intensities

Research Article
doi.org/10.1002/ejic.202300288

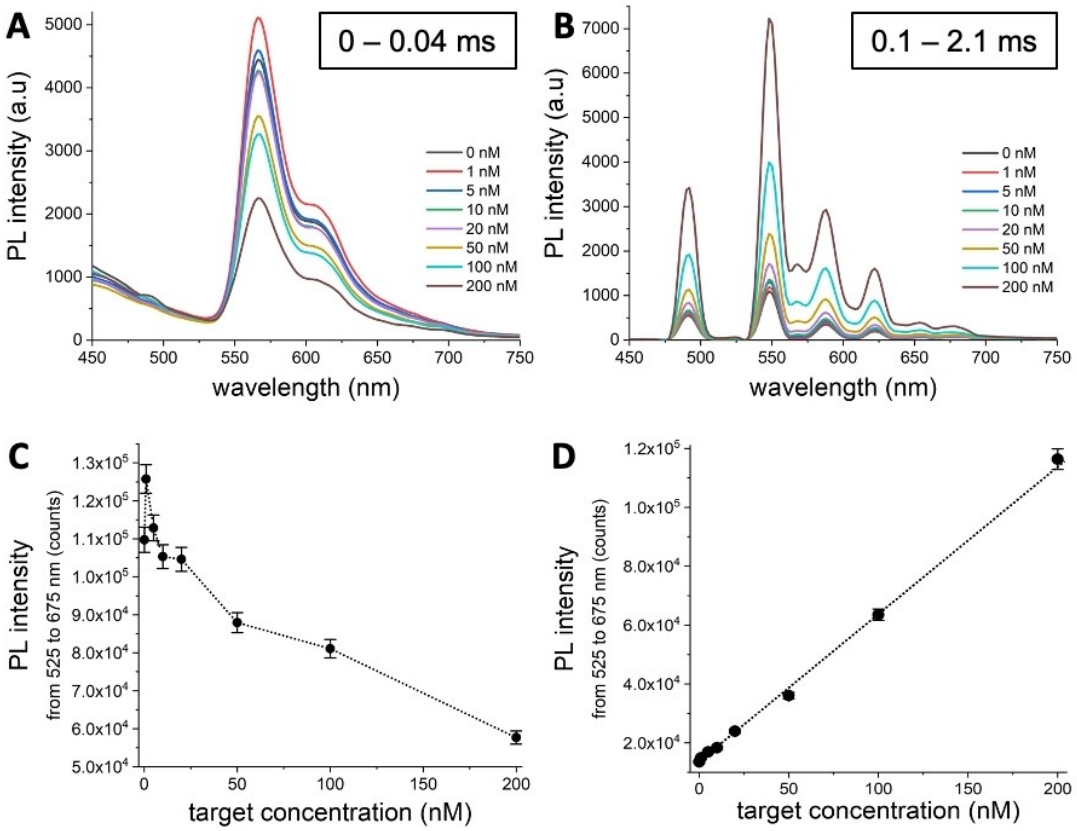

Figure 4. Target (miR-21) concentration-dependent TG PL intensities of the Tb-Cy3 TG-FRET MB in different TG windows recorded with specific delays and widths (0 delay and 40 μs width in A, 100 μs delay and 2.0 ms width in B) after pulsed excitation. The short window contains mainly acceptor components (A), whereas the long window contains both donor and acceptor components (B). In the short window, the PL intensities decrease with increasing target concentration (C). In the long window, the PL intensities increase with increasing target concentration (D).

in the two TG detection windows (Figure 5A). For all eight MLDs, the input state (0,0) consisted of a closed Tb-Cy3 TG-FRET MB (Figure 5B), which means that the output state was 1 for the short and 0 for the long output. NOR/OR, NAND/AND, XNOR/XOR, and IMPLEMENT/INHIBIT MLDs can then be realized by four different combinations of input DNAs (all with the same TG-FRET MB) that result in different outputs for the short/long TG detection windows. The schematic configurations and truth tables are shown in Figure 5 C to F. Clearly, the application of different and specific TG detection windows can significantly facilitate the design of biophotonic MLDs.

Physical unclonable functions (PUFs)

Security identification and authentication based on luminescence have reached very high levels of sophistication to improve security standards.[52,53] With the increase in computational power and the development of stronger models based on artificial intelligence, higher encryption and authentication security for the protection of genuine information and products or personal and classified data has become highly important. PUFs are physically or chemically generated objects that provide a specific physically defined output (the so-called response) for a defined input and condition (the so-called challenge).[54] The physical stimulus (challenge) creates an unpredictable but repeatable response and therefore, a challenge-response authentication via a specific challenge-response pair (CRP) is highly secure and it is virtually impossible to duplicate or clone a PUF (i.e., to decipher the security key). An ideal PUF must have an unpredictable response that changes significantly under even very small changes of the challenge and that is unique for a given challenge. The response should be simple to evaluate, impossible to model, and reveal no information about the physical or chemical structure of the PUF, which should still be simple and cheap in production.

Whereas PUFs are most often based on different materials, such as integrated circuits, randomized microscale patterns, or non-predictable electrical signals in semiconductor devices, biophotonic PUFs based on DNA and fluorescence have also been developed.[55] The nanoscale dimensions of DNA and the many diverse biological and optical materials and conditions make it intrinsically very difficult to impossible to replicate such PUFs. However, DNA-based photonic PUFs are usually quite complicated, e.g., by using a combination of DNA origami structures or other DNA networks and various different luminescent dyes and biomolecules, to establish a large variety of CRPs.

Our TG-FRET MBs are very simple (one DNA labeled with one lanthanide and one dye and one input DNA), extremely

Research Article
doi.org/10.1002/ejic.202300288

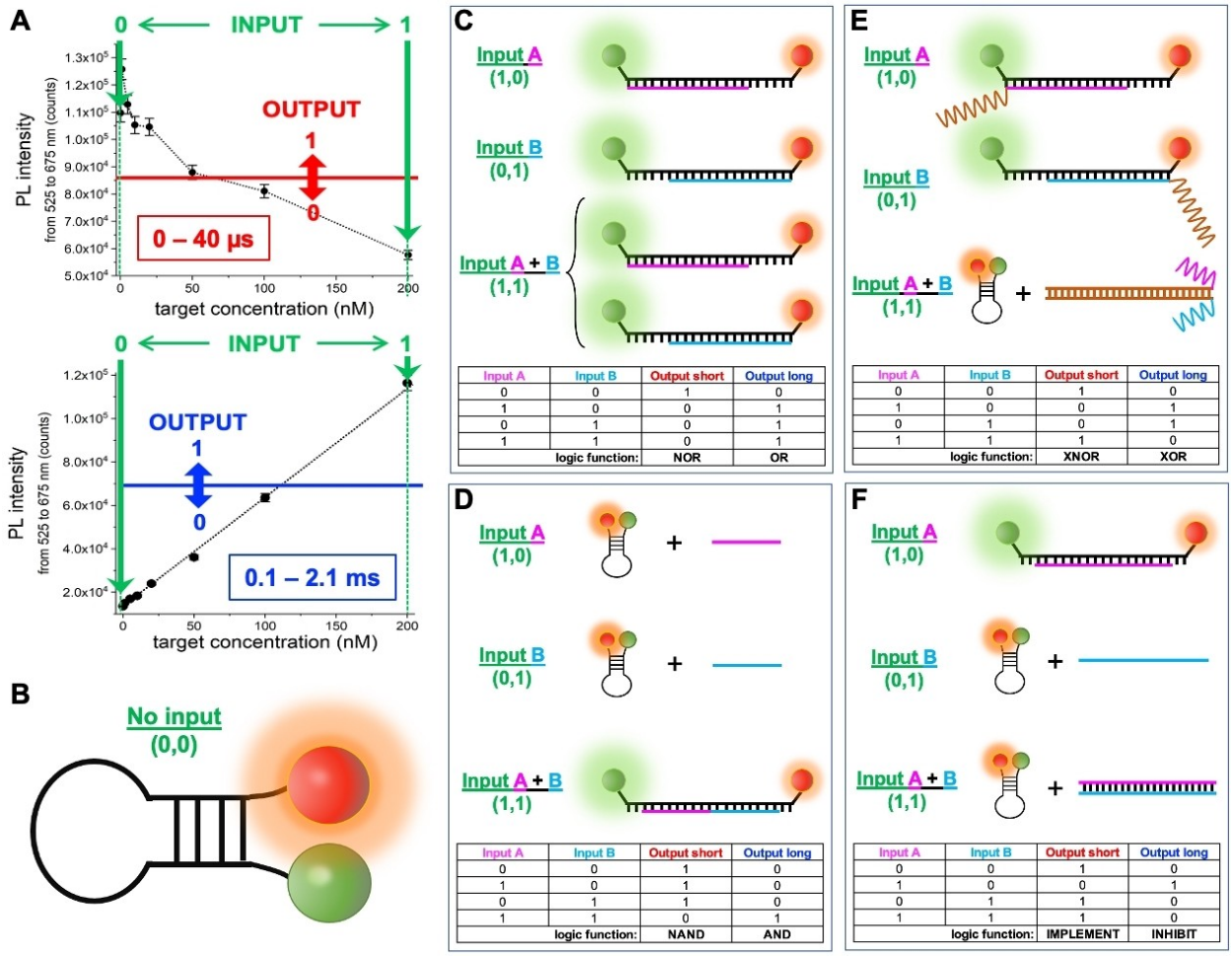

Figure 5. Concept of TG-FRET MB MLDs. A) Target concentration-dependent TG PL intensities in short (top) and long (bottom) detection windows can be used to define output intensities as 1 (on) or 0 (off). For MLDs, different DNAs can be used as biochemical inputs and the concentrations (e.g., 0 and 200 nM) can be defined as 0 or 1 input signals. Thus, 0 input would lead to 1/0 output and 1 input would lead to 0/1 output in the short/long TG detection window. B) The closed MB (no target) represents the (0,0) input, which results in 1 output for the short and 0 output for the long TG detection window. C to F) MB open (output 0/1 for short/long TG detection) and closed (output 1/0 for short/long TG detection) states depend on the addition of different DNA targets (A and B). Different target DNAs can be used to design distinct logic gates, which depend on the output selection and for which the truth tables are shown below the target-dependent opening and closing scenarios.

small (few nm) and thus, extremely hard to replicate without prior knowledge of the composition, and provide a large variety of input conditions (e.g., oligonucleotide concentration, buffer composition, temperature, wavelength, and time) and outputs (e.g., PL wavelength, intensity, and lifetime, and TG readout). This unique combination of simplicity and specific TG readout (same principles as used above for the MLDs) can add a new dimension to PUFs. An example of secure key code exchange via different TG-MB PUFs is shown in Figure 6. Although the variations of oligonucleotide concentrations, temperatures, and excitation wavelengths to accomplish distinguishable output signals are limited, more than 10^{18} (as shown in the example) CRPs can be created by fully exploiting the possible inputs and outputs mentioned above.

Conclusions

Despite the broad application of MB probes, lanthanide-to-quencher and lanthanide-to-dye TG-FRET MBs have been only rarely developed, investigated, or applied for biosensing. In particular, lanthanide-based MBs have only been used for the quantification of DNA and multiplexing concepts have been limited to the use of different acceptor dyes. Beyond biosensing, logic operations and security encryption have not been realized by TG-FRET MBs. Our study aimed at demonstrating a broader use of lanthanide-based TG-FRET MBs and we studied Tb-BHQ2 and Eu-BHQ2 lanthanide-quencher and Tb-Cy3 lanthanide-dye FRET pairs, which could quantify two different miRNA (miR-21 and miR-27) at low nanomolar concentrations and in a duplexed Tb-BHQ2/Eu-BHQ2 FRET format. Going a step beyond biosensing and exploiting the specific Tb-to-Cy3 distances in the closed and open MB state, we closely investigated the oligonucleotide target concentration-dependent PL intensities

Research Article
doi.org/10.1002/ejic.202300288

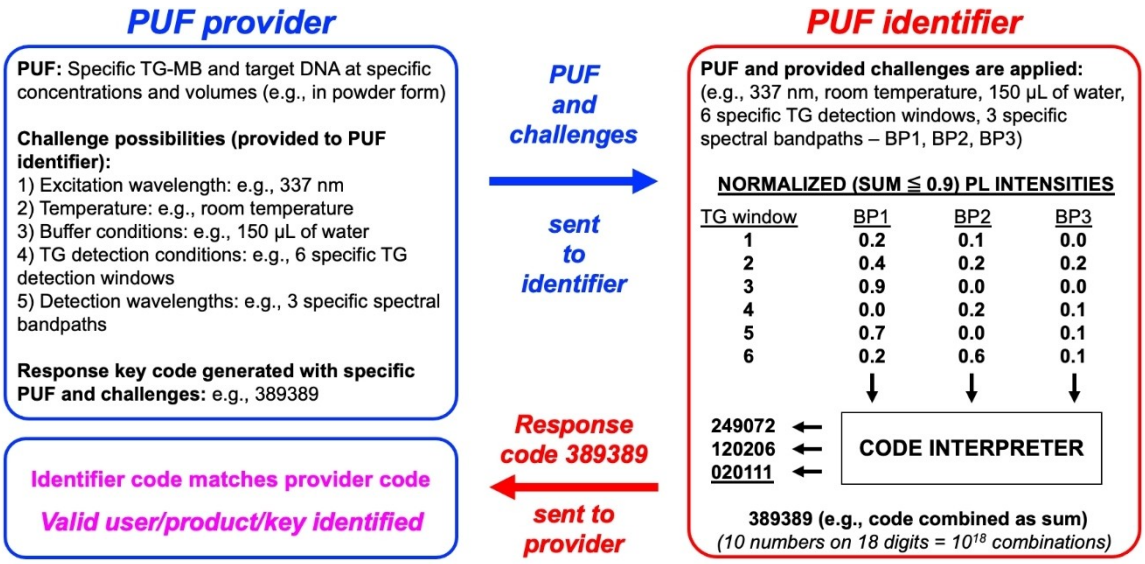

Figure 6. Example of information exchange, identification, or authentication via TG-FRET MBs. Security key code generation and exchange via a TG-FRET MB PUF and specific challenges and responses (CRP – challenge-response pairs). In the shown example with six TG detection windows and three spectral bandpasses, 18 digits with 10 different numbers from 0 to 9 can be created, which leads to 10^{18} different possible combinations. However, as shown in Figure S5, many more TG windows and spectral positions can be used to create even more code possibilities.

of the composed Tb and Cy3 PL spectra in different TG detection windows. The inverse direction (up or down) of the PL intensities in short and long TG detection windows with increasing target concentrations allowed for the design of various previously developed logic gates but with significantly less biochemical effort. Only half of the MB-target configurations were necessary because two different TG outputs could establish two logic gates with the same MB-target system. Finally, the almost unlimited choice of TG detection windows within the very long (~10 ms) PL decay of Tb and the distinct spectral features of Tb and Cy3, which result in unique spectral compositions in the 450 to 750 nm range for each distinct TG detection window, opened a new avenue for simple but highly secure biophotonic PUFs.

Although single wavelength detection of quenched lanthanides provides some benefits concerning simplicity, multiplexing based on changing the lanthanide donor is quite limited (limited available lanthanides that show bright emission in the visible wavelength range and significant overlap of their emission bands). A combination of Eu and Tb donors with different acceptors could possibly further extend the multiplexing capability beyond the duplexing demonstrated in our study. Also, miRNA quantification in the low nanomolar concentration range is maybe not sufficient for clinical diagnostics, for which picomolar of femtomolar LODs may be necessary. Therefore, our results concerning miRNA detection should be understood as a proof of concept to extend TG-FRET MBs to RNA quantification in general rather than an actual demonstration of miRNA-based clinical diagnostics. Such approaches would probably require DNA amplification and in that case the amplicons could possibly be detected via the lanthanide-based MBs. Also, the design concepts for MLDs and PUFs did not aim at demonstrating actual applications. Our objective was rather to show that the relatively simple TG-FRET MBs have a large potential to replace existing materials for such biophotonic computing and security tasks because they offer a much higher degree of simplicity without sacrificing biophotonic sophistication. Overall, we hope that our study can stimulate further research and development of lanthanide-based MB probes because we believe that they have much value for biophotonic applications that has been strongly underexplored until to date. In general, our study is another proof that lanthanide-based FRET is a highly versatile technology that provides specific spectral, temporal, and distance advantages that can only be realized by lanthanides.

Experimental Section

Materials and Methods

Reagents. BSA, bovine serum albumin (Sigma, cat.no. A9418). Custom MBs, and synthetic miR-21 and miR-27b (Eurogentec, custom oligonucleotides) are shown in Table 1. Store at −20 °C and avoid freeze-thaw cycles. For long-term storage −80 °C is recommended. Nuclease-free water (New England BioLabs, cat.no. B1500S). Sodium chloride (Sigma, cat.no. S9888). Magnesium chloride (Sigma, cat.no. M8266). HEPES (Sigma, cat.no. 54457). Trizma® hydrochloride (Sigma, cat.no. T3253). Lumi4Tb-NHS, Lumi804-Eu (Lumiphore). Newborn calf serum (Gibco).

Equipment. Electronic balance (Sartorius), thermal cycler (Eppendorf, mastercycler nexus x2), fluorescence plate reader (SPARK, TECAN), time-resolved fluorescence plate reader (DreamReader, Edinburgh Instrument), pH meter (Mettler Toledo), spectrometer (BMG Labtech), centrifuge (5424R, Eppendorf), Zeba Spin Desalting Columns 7 kDa MWCO (Thermo Fisher Scientific).

Förster distance calculation. Peak molar absorption coefficients of BHQ2 (38,000 $M^{-1}cm^{-1}$) and Cy3 (150,000 $M^{-1}cm^{-1}$) were used as

provided by the supplier. Förster distances (R_0) were calculated using the following equations:[56]

$$R_0 = 0.021\ (\kappa^2\ \Phi_D\ n^{-4}\ J)^{1/6}\ \text{nm} \quad (1)$$

$$J = \int_{450nm}^{700nm} I_D(\lambda)\ \varepsilon_A(\lambda)\ \lambda^4\ d\lambda \quad (2)$$

with the dipole-dipole orientation factor $\kappa^2 = 2/3$ (dynamic averaging regime, as justified by the random orientation of donor and acceptor during FRET and the long PL lifetime of Tb and Eu). The lanthanide-centered Tb and Eu PL quantum yields (Φ_D, provided by the supplier) were 0.7 and 0.46, respectively. The refractive index was $n = 1.35$ (aqueous solution). The overlap integral (J) was calculated by the spectral overlap between the area normalized (to unity) PL spectrum of the donor and the molar extinction coefficient ($M^{-1}cm^{-1}$) spectrum of the acceptor from 450 to 700 nm.

Reagent setup. Oligonucleotide solutions: resuspend custom oligonucleotides (beacon probes, synthetic miRNAs) in nuclease-free water to 100 μM concentration, store at −20 °C, and avoid freeze-thaw cycles. Hybridization Buffer (HB): 20 mM Tris–Cl, 500 mM NaCl, 2 mM $MgCl_2$, 0.1% BSA, pH 8.0 at 25 °C. 100 mM HEPES buffer, pH 7.4 at 25 °C. 100 mM Carbonate buffer, pH 9 at 25 °C.

Tb and Eu oligonucleotide conjugation. Lanthanide–oligonucleotide (Tb or Eu-oligo) conjugation was performed as described earlier.[34] In brief, 2.1 μL of 8 mM Lumi4Tb-NHS or Lumi804-Eu (in anhydrous DMF) was mixed with 10 μL of 100 μM amino-functionalized oligonucleotide and 7.9 μL of 100 mM carbonate buffer pH 9 at 25 °C. In the presented mixture, the lanthanide complex is in a ca. 16-fold molar excess over the oligonucleotide. The mixture was incubated overnight at 4 °C. The Tb (Eu)-oligo conjugates were purified 3 times using Zeba Spin Desalting Columns (7 kDa MWCO) following the desalting protocol provided by the supplier. The concentration of conjugated oligonucleotides was calculated by absorption measurement using a BMG labtech spectrometer in the 200–800 nm range, absorption peaks at 260 nm, 340 nm, 363 nm, 550 nm, and 600 nm correspond to oligonucleotide, terbium, europium, Cy3, and BHQ2, respectively. Corresponding absorption spectra shown in Figure 1A.

To ensure that all beacon probes are in the closed hairpin state, a preparation heating protocol was applied for all MB probes after Tb/Eu conjugation. The protocol involves heating to 95 °C for 5 minutes, followed by a gradual decrease in temperature to 22 °C at a rate of 2 °C per minute. After this preparation procedure, MBs were applied for the assays listed below.

Assays

Optimization of experimental conditions. To optimize temperature conditions for the best assay performance, various incubation temperature protocols were applied. 25 μL of 240 nM Tb-BHQ2 beacon probe in hybridization buffer (HB) was mixed with 25 μL of target miR-21 in various concentrations (0–200 nM), followed by adding 50 μL of HB. Mixtures were incubated in three different conditions: a) 45 minutes at room temperature, b) 45 minutes at 37 °C, c) heat to 65 °C for 10 minutes and then decrease the temperature to 22 °C by 2 °C/minute (~45 minutes). Each concentration was prepared in three repeats ($n = 3$).

Tb-BHQ2/Tb-Cy3/Eu-BHQ2 assay performance for miRs detection (calibration test, LOD test). The mixture of 50 μL of 200 nM beacon probe (Tb-BHQ2 or Tb-Cy3 or Eu-BHQ2) in HB, 25 μL of complimentary miRs target (miR-21, miR-27b) in various concentrations from 0 (blank) to 200 nM, and 25 μL of HB were incubated using the Assay protocol below. Each concentration was prepared in three repeats ($n = 3$), except blank, for which 10 repeats were used ($n = 10$). The Tb-BHQ2 and Eu-BHQ2 assays were analyzed using relative TG PL intensities (TG PL intensity at a given target concentration divided by TG PL intensity without target) of Tb or Eu:

$$\begin{aligned} \textbf{Tb}:\ rel.\ PL\ intensity &= \frac{I_{Tb\ (c=x)}}{I_{Tb\ (c=0)}} \\ \textbf{Eu}:\ rel.\ PL\ intensity &= \frac{I_{Eu\ (c=x)}}{I_{Eu\ (c=0)}} \end{aligned} \quad (3)$$

The Tb-Cy3 assays were analyzed using the relative FRET ratio of the TG PL intensity of the Cy3 acceptor (at 570 nm) and the TG PL intensity of the Tb donor (at 494 nm):

$$\begin{aligned} FRET\ ratio &= \frac{I_{Cy3\ (c=x)}}{I_{Tb\ (c=x)}} \\ rel.\ FRET\ ratio &= \frac{FRET\ ratio\ (c=x)}{FRET\ ratio\ (c=0)} \end{aligned} \quad (4)$$

Specificity tests: 50 μL of 200 nM Tb-BHQ2 MB in HB, 25 μL of target or non-target miR at concentrations up to 200 nM, and 25 μL of HB were incubated using the Assay protocol below. Non-specific miR targets did not result in significant signals (data not shown).

Duplexed homogeneous TG-FRET MB assay. The mixture of 50 μL of 200 nM MBs (Tb-BHQ2 and Eu-BHQ2) in HB and 25 μL of each miR-21 and miR-27b target in various concentrations from 0 (blank) to 200 nM was incubated using the Assay protocol below. Each concentration was prepared in duplicates. Calibration curve: the mixture of 50 μL of 200 nM MB (Tb-BHQ2 and Eu-BHQ2) in HB, 25 μL of miR-21 or miR-27b target in various concentrations from 0 (blank) to 200 nM, and 25 μL of HB was incubated using the Assay protocol below. TG intensity was measured for the major peaks of the lanthanides emission at 550 ± 2.5 nm (for Tb-BHQ2) and 620 ± 2.5 nm (for Eu-BHQ2).

Correction coefficient for Eu-BHQ2 in mixture with Tb was calculated as:

$$Eu - BHQ2\ coef = 1 - \frac{I_{Tb\ (620\ nm)}}{I_{Eu\ (620\ nm)}} = 0.755 \quad (5)$$

Correction coefficient for Tb-BHQ2 in mixture with Eu was calculated as:

$$Tb - BHQ2\ coef = 1 - \frac{I_{Eu\ (550\ nm)}}{I_{Tb\ (550\ nm)}} = 0.998 \quad (6)$$

This value was very close to unity and thus, correction was not applied.

Spike-in test with newborn calf serum (NBCS). Control calibration curve (marked as 0): mixture of 50 μL of 200 nM MB Tb-BHQ2 in HB, 25 μL of miRs target (miR-21) in various concentrations from 0 to 200 nM, and 25 μL of HB; 20% calibration curve: mixture of 50 μL of 200 nM MB in HB, 25 μL of miRs target in various concentrations from 0 to 200 nM, 20 μL of HB, and 5 μL of NBCS; 50% calibration curve: mixture of 50 μL of 200 nM MB in HB, 25 μL of miRs target in various concentrations from 0 to 200 nM, 12.5 μL of HB, and 12.5 μL of NBCS; 100% calibration curve: mixture of 50 μL of 200 nM MB in

HB, 25 μL of miRs target in various concentrations from 0 to 200 nM, and 25 μL of NBCS. Each concentration was prepared in 4 repeats ($n=4$). The mixtures were incubated using the Assay protocol below.

Assay protocol. All assays were performed under the same experimental conditions and measurement parameters unless otherwise indicated. Mixtures from all assays were incubated using the following protocol: heat to 65 °C for 10 minutes and then decrease the temperature to 22 °C by 2 °C/minute. After incubation, 90 μL of the reaction mixture was transferred to a 96-well black plate and PL intensity was measured on a SPARK fluorescence plate reader with the following parameters: TG intensity protocol-excitation 337 ± 10 nm (363 ± 10 for Eu), emission 494 ± 2.5 nm (for Tb) or 570 ± 2.5 nm (for Cy3 dye) or 620 ± 2.5 (for Eu-BHQ2), lag time (μs) 100, integration time (μs) 2000. For the duplexed assays, integration time was 1000 μs.

PL intensity scan and decay curves measurements. The calibration curves with various target concentrations were prepared as described in the calibration test section. After incubation, 90 μL of the reaction mixture was transferred to a 96-well black plate and PL intensity was measured on a SPARK fluorescence plate reader with the following parameters: TG intensity protocol-excitation 337 ± 10 nm, emission 440–750 nm, lag time (μs) varied from 0 to 100, integration time (μs) varied from 20 to 2000, gain 100. Decay curves were measured on DreamReader time-resolved fluorescence plate reader in a time range from 0 to 8 ms, laser excitation 337 nm, PL intensity detection using bandpass optical filters 494 ± 20, 567 ± 7.5, 605 ± 7.5, 620 ± 4, 640 ± 7 (Semrock).

Supporting Information

The Supporting information is available as PDF file. Variation of the incubation temperature (Figure S1); Target concentration-dependent PL decay curves (Figure S2); Determination of LODs (Figure S3); Spike-in test with NBCS (Figure S4); Development of TG PL spectra over time (Figure S5).

Acknowledgements

We thank Lumiphore, Inc. for the gift of Lumi804 and Lumi4 reagents. This work was supported by the Institut National du Cancer and the Direction Générale de l'Offre de Soins (INCa and DGOS; project PRTk 16158-Gynomir), ITMO Cancer of Aviesan within the framework of the 2021–2030 Cancer Control Strategy through funds administered by Inserm (project "ACTION"), the Polish Academy of Sciences and the European Commission (H2020-MSCA-COFUND-2018) under the Marie Skłodowska-Curie grant agreement No 847639 (PASIFIC), the Brain Pool program funded by the Ministry of Science and ICT through the National Research Foundation of Korea (2021H1D3A2A02049589), Seoul National University, Université de Rouen Normandie, Normandie Université, INSA Rouen, CNRS, European Regional Development Fund, Labex SynOrg (ANR-11-LABX-0029), Carnot Institute I2C, XL-Chem graduate school (ANR-18-EURE-0020 XL-CHEM), and the Région Normandie.

Conflict of Interests

The authors declare no conflict of interest.

Data Availability Statement

The data that support the findings of this study are available in the supplementary material of this article and at the authors upon request.

Keywords: FRET · terbium · europium · clinical diagnostics · molecular logic devices · encryption

[1] R. M. Clegg, in *Laboratory Techniques in Biochemistry and Molecular Biology*, Elsevier, **2009**, pp. 1–57.
[2] G. Bunt, F. S. Wouters, *Biophys. Rev. Lett.* **2017**, *9*, 119–129.
[3] I. L. Medintz, N. Hildebrandt, Eds., *FRET – Förster Resonance Energy Transfer: From Theory to Applications*, John Wiley & Sons, **2013**.
[4] J. M. Zwier, N. Hildebrandt, in *Reviews in Fluorescence 2016* (Ed.: Geddes, CD), Springer, Cham, **2017**, pp. 17–43.
[5] W. R. Algar, N. Hildebrandt, S. S. Vogel, I. L. Medintz, *Nat. Methods* **2019**, *16*, 815–829.
[6] K. E. Sapsford, B. Wildt, A. Mariani, A. B. Yeatts, I. Medintz, in *FRET – Förster Resonance Energy Transfer*, John Wiley & Sons, Ltd, **2013**, pp. 165–268.
[7] C. Chen, N. Hildebrandt, *TrAC Trends Anal. Chem.* **2020**, *123*, 115748.
[8] L. Francés-Soriano, N. Hildebrandt, L. J. Charbonnière, in *Comprehensive Inorganic Chemistry III (Third Edition)* (Eds.: J. Reedijk, K. R. Poeppelmeier), Elsevier, Oxford, **2023**, pp. 486–510.
[9] M. Matulionyte, A. Skripka, A. Ramos-Guerra, A. Benayas, F. Vetrone, *Chem. Rev.* **2022**, *123*, 515–554.
[10] G. Sun, Y. Xie, L. Sun, H. Zhang, *Nanoscale Horiz.* **2021**, *6*, 766–780.
[11] T. J. Sørensen, S. Faulkner, in *Metal Ions in Bio-Imaging Techniques* (Eds.: A. Sigel, E. Freisinger, R. K. O. Sigel), De Gruyter Berlin, **2021**.
[12] H. Li, X. Wang, T. Y. Ohulchanskyy, G. Chen, *Adv. Mater.* **2021**, *33*, 2000678.
[13] Z. Zhang, Q. Han, J. W. Lau, B. Xing, *ACS Materials Lett.* **2020**, *2*, 1516–1531.
[14] J.-C. G. Bünzli, *Eur. J. Inorg. Chem.* **2017**, *2017*, 5058–5063.
[15] M. Sy, A. Nonat, N. Hildebrandt, L. J. Charbonniere, *Chem. Commun.* **2016**, *52*, 5080–5095.
[16] J.-C. G. Bünzli, *Coord. Chem. Rev.* **2015**, *293–294*, 19–47.
[17] S. A. Díaz, G. Lasarte-Aragones, R. G. Lowery, Aniket, J. N. Vranish, W. P. Klein, K. Susumu, I. L. Medintz, *ACS Appl. Nano Mater.* **2018**, *1*, 3006–3014.
[18] S. Wheeler, S. J. Butler, *Anal. Sens.* **2023**, *3*, e202200036.
[19] X. Qiu, J. Xu, M. Cardoso Dos Santos, N. Hildebrandt, *Acc. Chem. Res.* **2022**, *55*, 551–564.
[20] N. Hildebrandt, K. D. Wegner, W. R. Algar, *Coord. Chem. Rev.* **2014**, *273–274*, 125–138.
[21] S. I. Weissman, *J. Chem. Phys.* **1942**, *10*, 214–217.
[22] G. A. Crosby, R. E. Whan, R. M. Alire, *J. Chem. Phys.* **1961**, *34*, 743–748.
[23] D. L. Dexter, *J. Chem. Phys.* **1953**, *21*, 836–850.
[24] G. Chatel, M. Caron, J. Padros, https://bioauxilium.com/wp-content/uploads/2021/03/BioAuxilium-Application-Notes-Kit-comparison.pdf**2022**.
[25] J. Lahdenperä, J. Karvinen, P. Kivelä, https://resources.perkinelmer.com/lab-solutions/resources/docs/app_sensitivity_dynamic_range_microplates.pdf**2004**.
[26] A. Ylikoski, A. Elomaa, P. Ollikka, H. Hakala, V.-M. Mukkala, J. Hovinen, I. Hemmilä, *Clin. Chem.* **2004**, *50*, 1943–1947.
[27] H. Bazin, E. Trinquet, G. Mathis, *Rev. Mol. Biotechnol.* **2002**, *82*, 233–250.
[28] G. Mathis, *J. Biomol. Screening* **1999**, *4*, 309–313.
[29] I. Hemmila, *J. Biomol. Screening* **1999**, *4*, 303–307.
[30] H.-J. Fu, R. Su, L. Luo, Z.-J. Chen, T. J. Sørensen, N. Hildebrandt, Z.-L. Xu, *ACS Sens.* **2022**, *7*, 1113–1121.
[31] X. Qiu, J. Guo, J. Xu, N. Hildebrandt, *J. Phys. Chem. Lett.* **2018**, *9*, 4379–4384.

[32] M. Massey, M. G. Ancona, I. L. Medintz, W. R. Algar, *ACS Photonics* **2015**, *2*, 639–652.
[33] M. Massey, I. L. Medintz, M. G. Ancona, W. R. Algar, *ACS Sens.* **2017**, *2*, 1205–1214.
[34] M. Dekaliuk, P. Busson, N. Hildebrandt, *Anal. Sens.* **2022**, *2*, e202200049.
[35] J. Xu, X. Qiu, N. Hildebrandt, *Nano Lett.* **2021**, *21*, 4802–4808.
[36] J. Xu, J. Guo, N. Golob-Schwarzl, J. Haybaeck, X. Qiu, N. Hildebrandt, *ACS Sens.* **2020**, *5*, 1768–1776.
[37] J. Guo, C. Mingoes, X. Qiu, N. Hildebrandt, *Anal. Chem.* **2019**, *91*, 3101–3109.
[38] M. Dekaliuk, X. Qiu, F. Troalen, P. Busson, N. Hildebrandt, *ACS Sens.* **2019**, *4*, 2786–2793.
[39] X. Qiu, J. Xu, J. Guo, A. Yahia-Ammar, N.-I. Kapetanakis, I. Duroux-Richard, J. J. Unterluggauer, N. Golob-Schwarzl, C. Regeard, C. Uzan, S. Gouy, M. DuBow, J. Haybaeck, F. Apparailly, P. Busson, N. Hildebrandt, *Chem. Sci.* **2018**, *9*, 8046–8055.
[40] S. Tyagi, F. R. Kramer, *Nat. Biotechnol.* **1996**, *14*, 303–308.
[41] J. Zheng, R. Yang, M. Shi, C. Wu, X. Fang, Y. Li, J. Li, W. Tan, *Chem. Soc. Rev.* **2015**, *44*, 3036–3055.
[42] L. N. Krasnoperov, S. A. E. Marras, M. Kozlov, L. Wirpsza, A. Mustaev, *Bioconjugate Chem.* **2010**, *21*, 319–327.
[43] V. Laitala, A. Ylikoski, H.-M. Raussi, P. Ollikka, I. Hemmilä, *Anal. Biochem.* **2007**, *361*, 126–131.
[44] M. Massey, M. G. Ancona, I. L. Medintz, W. R. Algar, *Anal. Chem.* **2015**, *87*, 11923–11931.
[45] D. D. Root, C. Vaccaro, Z. Zhang, M. Castro, *Biopolymers* **2004**, *75*, 60–70.
[46] M. K. Johansson, R. M. Cook, J. Xu, K. N. Raymond, *J. Am. Chem. Soc.* **2004**, *126*, 16451–16455.
[47] J. Li, W. Zhou, X. Ouyang, H. Yu, R. Yang, W. Tan, J. Yuan, *Anal. Chem.* **2011**, *83*, 1356–1362.
[48] A. M. James, M. B. Baker, G. Bao, C. D. Searles, *Theranostics* **2017**, *7*, 634–646.
[49] J. Guo, X. Qiu, C. Mingoes, J. R. Deschamps, K. Susumu, I. L. Medintz, N. Hildebrandt, *ACS Nano* **2019**, *13*, 505–514.
[50] K. S. Park, M. W. Seo, C. Jung, J. Y. Lee, H. G. Park, *Small* **2012**, *8*, 2203–2212.
[51] J. C. Claussen, W. R. Algar, N. Hildebrandt, K. Susumu, M. G. Ancona, I. L. Medintz, *Nanoscale* **2013**, *5*, 12156–12170.
[52] V. Nellore, S. Xi, C. Dwyer, *ACS Nano* **2015**, *9*, 11840–11848.
[53] C. Dubey, A. Yadav, D. Baloni, S. Singh, A. K. Singh, S. K. Singh, A. K. Singh, *Methods Appl. Fluoresc.* **2023**, *11*, 025001.
[54] R. Arppe, T. J. Sørensen, *Nat. Chem. Rev.* **2017**, *1*, 1–13.
[55] W. P. Klein, S. A. Díaz, M. Chiriboga, S. A. Walper, I. L. Medintz, *ACS Appl. Nano Mater.* **2019**, *2*, 7459–7465.
[56] N. Hildebrandt, in *FRET – Förster Resonance Energy Transfer: From Theory to Applications* (Eds.: I. Medintz, N. Hildebrandt), Wiley VCH, Weinheim, **2013**, pp. 105–164.

Manuscript received: May 16, 2023
Revised manuscript received: August 24, 2023
Accepted manuscript online: September 1, 2023
Version of record online: September 18, 2023